Dynamics of a Dark Matter Field with a Quartic Self-Interaction Potential

P. J. E. Peebles
Joseph Henry Laboratories, Princeton University, Princeton NJ 08544
(February 5, 2008)

It may prove useful in cosmology to understand the behavior of the energy distribution in a scalar field that interacts only with gravity and with itself by a pure quartic potential, because if such a field existed it would be gravitationally produced, as a squeezed state, during inflation. It is known that the mean energy density in such a field after inflation varies with the expansion of the universe in the same way as radiation. I show that if the field initially is close to homogeneous, with energy density contrast $|\delta\rho/\rho| \ll 1$ and coherence length L, the energy density fluctuations behave like acoustic oscillations in an ideal relativistic fluid for a time on the order of $L/|\delta\rho/\rho|$. This ends with the appearance of features that resemble shock waves but interact in a close to elastic way that reversibly disturbs the energy distribution.

I. INTRODUCTION

The dark matter that in standard physics dominates the mass of the universe might have originated in the same way as ordinary matter and radiation, in reactions at high redshift, or some or all of it might have been gravitationally produced by inflation [1], [2]. A simple example of the latter is a single scalar field $y(\mathbf{x}, t)$ with the pure quartic self-interaction potential

$$V = \lambda y^4/4, \tag{1}$$

minimal coupling to gravity, and no other interactions. This could not be the dark matter that is gravitationally bound to galaxies and clusters of galaxies, but it might have an observationally interesting effect on structure formation. A model based on the idea that the primeval fluctuations in this y-field energy distribution broke homogeneity to seed structure formation is compared to the measured power spectra of the radiation and matter distributions in [3]. Here I consider some aspects of the evolution of the y-field energy distribution.

Ford [4] and Turner [5] show that after inflation ends the energy density in a homogeneous field with the quartic potential in Eq (1) scales with the cosmological expansion parameter as $\rho_y \propto a(t)^{-4}$, the same as for radiation. This is important because it means the y-field energy could be large enough when inflation ends to be a significant perturbation to the energy distribution, yet small enough thereafter that it does not interfere with the standard models for light element production at redshift $z \sim 10^{10}$ and structure formation at lower redshift. It may be significant also that the parameter λ in the quartic potential can be chosen so that eternal inflation gravitationally produces a potentially interesting value for the energy density ρ_y. There is the danger noted by Felder, Kofman and Linde [6] that gravitational production can make ρ_y the dominant energy density, so this field assumes the role of the inflaton. Peebles and Vilenkin [2] show that in eternal inflation, with the quartic inflaton potential $V_\phi = \lambda_\phi \phi^4/4$, this problem does not arise if the y-field parameter satisfies $\lambda_\phi \ll \lambda$.

Since the mean value of ρ_y after inflation varies in the like radiation it might not seem surprising that energy density fluctuations can behave in a similar way. An early step in this direction was taken by Khlopov, Malomed, and Zel'dovich [7], who note that the quartic potential with positive λ produces a positive effective pressure. Other steps toward the fluid picture are reviewed in Section II. A linear acoustic wave model for the evolution of small spatial fluctuations in the field energy density can only be an approximation: the numerical solution of Khlebnikov & Tkachev [8] shows the transfer of fluctuations in the spatial distribution of the energy to higher wavenumbers that Gruzinov [9] remarks can be interpreted as the relaxation to equipartition of the kinetic, gradient and potential energies. The purpose of this paper is to find a description of the onset of the departure from the acoustic wave model.

This analysis assumes $\partial y/\partial t = 0$ at the end of inflation, as follows from gravitational production of y, and the field value is close to homogeneous. Peebles and Vilenkin [2] show this last assumption is a good approximation across the present Hubble length if $\lambda \lesssim 0.01$. Khlopov, Malomed, and Zel'dovich [7] study the gravitational effect of the evolution of the energy distribution in a scalar field with quartic plus quadratic self-interaction potential, in a WKB approximation. Here I consider a pure quartic potential, where the effect of the peculiar gravitational acceleration is likely to be important only near black holes. I accordingly use an expanding spacetime that is homogeneous and isotropic. The y-field is supposed to have been squeezed by inflation to very large occupation numbers, so it can be treated as a classical field.

II. PRELIMINARY REMARKS

When the field is exactly homogeneous, the field equation in Minkowski spacetime can be scaled to a one-dimensional oscillator,

$$\ddot\eta = -\eta^3, \qquad -1 \le \eta \le 1, \tag{2}$$

where $\dot y = \partial y/\partial t$, t is proper world time, and $\eta(t)$ has unit amplitude. Following Ford [4], one arrives at a virial relation by multiplying Eq. (2) by η and averaging over time. The left hand side is $\eta\ddot\eta = d(\eta\dot\eta)/dt - \dot\eta^2$; in the average over time large compared to the oscillator period the second term is dominant, giving [4], [10]

$$\langle\dot\eta^2\rangle = \langle\eta^4\rangle = 1/3, \tag{3}$$

where the energy is $\dot\eta^2/2+\eta^4/4 = 1/4$ for unit amplitude. Greene *et al.* [10] show $\eta(t)$ has frequency

$$\omega = 2\pi^{3/2}\Gamma(1/4)^{-2} = 0.847\ldots. \tag{4}$$

The scaling to potential $\lambda y^4/4$ and amplitude y_o is

$$y = y_o\eta(\lambda^{1/2}y_o t), \qquad \omega = 0.847\lambda^{1/2}y_o. \tag{5}$$

Turner [5] notes that when the field is spatially homogeneous, $y = y(t)$, with amplitude y_o, the time average of the stress-energy tensor T_i^j is diagonal with $\rho = \dot y^2/2 + \lambda y^4/4 = \lambda\langle y_o^4\rangle/4$ and $p = \langle\dot y^2/2 - \lambda y^4/4\rangle = \lambda\langle y_o^4/12\rangle$, the time averages following from Eq. (3). The ratio p/ρ is the same as for an ideal relativistic fluid. One sees from the vanishing of the covariant divergence of this diagonal stress-energy tensor in comoving coordinates that the energy density scales with the cosmological expansion parameter as

$$\rho \propto a(t)^{-4}. \tag{6}$$

Other derivations are given by Ford [4] and Turner [5].

If the field is inhomogeneous the action with quartic potential is simplified by changing from proper time t to conformal time $\tilde t = \int dt/a$ and letting $\tilde y = ay$. When $\omega \gg \dot a/a$ this brings the action for $\tilde y$ to the Minkowski form. In this limit a solution $\tilde y(\tilde t, \mathbf{x})$ to the Minkowski problem, that has fixed mean energy density, produces a solution $y(t, \mathbf{x})$ in which the kinetic, gradient and potential energy densities all scale as $a(t)^{-4}$ relative to the Minkowski solution. The mean energy density thus satisfies Eq. (6) (eg. [2], [11]).

One gets some feeling for the evolution of the energy distribution in an inhomogeneous solution by starting from the homogeneous solution obtained by a Lorentz transformation of Eq. (5),

$$y(\mathbf{r}, t) = y_o\eta(\lambda^{1/2}y_o\gamma(t - \mathbf{v}\cdot\mathbf{r})). \tag{7}$$

The time average of the stress-energy tensor T_{ij} in this solution is the same as for an ideal relativistic fluid with streaming velocity $\mathbf{v}$, as one sees from the Lorentz transformation from T_{ij} for $y = y(t)$ or by computing T_{ij} for $y(\mathbf{r}, t)$ in Eq. (7). If the field initially is locally well approximated by Eq. (7), with amplitude y_o and velocity $\mathbf{v}$ that vary slowly with position, then T_{ij} is close to the stress-energy tensor of an inhomogeneous relativistic ideal fluid, and the vanishing divergence of T_{ij} tells us the energy starts to redistribute itself in the manner of a relativistic fluid. (This was pointed out to me by Vilenkin [12]). The analysis in the next section is meant to find indications of how long this fluid approximation might last.

The discussion conveniently begins with yet another demonstration of the evolution of the mean energy density in Eq. (6) when the field is inhomogeneous. The wave equation is

$$\frac{\partial^2 y}{\partial t^2} + 3\frac{\dot a}{a}\frac{\partial y}{\partial t} = \frac{\nabla^2 y}{a^2} - \lambda y^3, \tag{8}$$

and the energy density and flux are

$$\rho = \dot y^2/2 + (\nabla y)^2/2a^2 + \lambda y^4/4, \qquad \mathbf{f} = -\dot y\nabla y/a, \tag{9}$$

where the space derivatives are with respect to coordinate distance x and adx is a proper length. The energy conservation equation is

$$\partial\rho/\partial t + \nabla\cdot f/a = -[3\dot y^2 + (\nabla y)^2/a^2]\dot a/a. \tag{10}$$

As in Eq. (3), the result of multiplying Eq. (8) by y and averaging over space and over a time interval large compared to the period ω^{-1} of oscillation of y and small compared to the expansion time $a/\dot a$ is the virial relation

$$\langle\dot y^2\rangle = \langle(\nabla y)^2\rangle/a^2 + \lambda\langle y^4\rangle. \tag{11}$$

This brings the mean energy density to

$$\langle\rho\rangle = 3\langle\dot y^2\rangle/4 + \langle\nabla y^2\rangle/4a^2. \tag{12}$$

The space average of Eq. (10) eliminates the energy flux density, and with Eq. (12) we get $\langle\rho\rangle \propto a(t)^{-4}$.

If the sum of the kinetic and gradient energy densities is large compared to the potential energy then y has the familiar properties of a free massless field: initial large-scale fluctuations in the energy distribution grow smoother as in free streaming of a gas of relativistic particles. In the situation to be discussed next the initially small gradient energy density grows larger in patches and may eventually become comparable to the kinetic and potential energies. In this case large-scale density fluctuations would evolve like a relativistic gas of massless particles with mean free path comparable to a characteristic de Broglie wavelength.

The model presented in the next section is meant to describe the onset of this cascade to larger wavenumbers, when the field gradient energy density is small compared to the kinetic plus potential energy densities. The examples in Section IV show that numerical solutions to this model are in satisfactory agreement with the energy distributions from numerical solutions of the wave equation. Both demonstrate the failure of the linear acoustic wave model for the behavior of fluctuations in the energy distribution, in the development of features that resemble shock waves except that they pass each other in a nearly free way.

III. THE WEAK GRADIENT MODEL

Since the period of oscillation of y scales inversely with the amplitude (Eq. 5), an initial gradient of the amplitude produces a growing gradient of the phase of the oscillation. This makes the field an oscillating function of position, as in Eq. (7), and produces energy flux $\mathbf{f}$ that tends to carry energy from maxima toward minima of the distribution. When the field gradient is on the order of $\nabla y \sim v\dot{y}$ the streaming velocity in this rearrangement of the energy is $\sim f/\rho \sim v$. In acoustic waves in a relativistic fluid v is small when the density fluctuations are small, $|\delta\rho/\rho| \ll 1$. Following this condition, the weak gradient model (WGM) for the energy distribution in the y-field assumes two inequalities. First, the period $\sim \omega^{-1}$ of oscillation of the field is much shorter than the wavelength $\sim (v\omega)^{-1}$ of spatial oscillations, because $v \ll 1$. Second, the wavelength of field oscillations is much shorter than the coherence length L of the energy distribution. That is, the WGM assumes $\omega \gg \omega v \gg 1/L$.

The goal is to study the redistribution of energy on the scale of L, not the more rapid oscillations of y in space and time, so the energy density and flux are smoothed over a window in spacetime that is large compared to the latter and small compared to L. The virial relation in Eq (11) applies to the averages over this intermediate scale, and the smoothed energy distribution accordingly satisfies Eq. (12). The same smoothing of the energy Eq. (10) with Eq. (12) yields

$$\partial\langle\rho\rangle/\partial t + \nabla\cdot\langle\mathbf{f}\rangle/a = -4\langle\rho\rangle\dot{a}/a. \tag{13}$$

The angular brackets mean the result of this smoothing.

Eq. (13) is the first relation in the WGM. The second follows by writing out the time derivative of the energy flux density (Eq. 9) and using the wave Eq. (8):

$$\frac{\partial\mathbf{f}}{\partial t} + 4\mathbf{f}\frac{\dot{a}}{a} = \frac{1}{a}\nabla\left(\frac{1}{4}\lambda y^4 - \frac{1}{2}\dot{y}^2)\right) - \frac{1}{a^3}\nabla y\nabla^2 y. \tag{14}$$

Eq (12) brings the mean of the first term on the right hand side to

$$\langle\lambda y^4/4 - \dot{y}^2/2\rangle = -\langle\rho\rangle/3 - \langle(\nabla y)^2\rangle/(6a^2). \tag{15}$$

The last term is simplified by noting that the energy flux density satisfies

$$\mathbf{f}\nabla\cdot\mathbf{f} = \frac{1}{a^2}\dot{y}^2\nabla y\nabla^2 y - \frac{1}{2a}\mathbf{f}\frac{\partial(\nabla y)^2}{\partial t}. \tag{16}$$

Eq. (16) and the second term on the right hand side of Eq. (15) will serve as small corrections to a wave equation for ρ and $\mathbf{f}$, so I approximate these parts by their forms for a homogeneous energy distribution with streaming velocity $\mathbf{v}$. Eq. (7) with $v \ll 1$ says $\nabla y/a \cong -\mathbf{v}\dot{y}$. With $\langle\dot{y}^2\rangle \cong 4\langle\rho\rangle/3$ the energy flux density is $\langle\mathbf{f}\rangle \cong 4\langle\rho\rangle\mathbf{v}/3$. Thus in the last term in Eq. (15) we have

$$\langle(\nabla y)^2\rangle/a^2 \cong (3/4)f^2/\rho. \tag{17}$$

The last term on the right hand side of Eq. (16) is on the order of v^2 times the left hand side, and so is discarded. In these approximations Eq. (14) becomes

$$\frac{\partial\mathbf{f}}{\partial t} + 4\frac{\dot{a}}{a}\mathbf{f} = -\frac{1}{3a}\nabla\rho - \frac{1}{8a\rho}\nabla f^2 - \frac{3}{4\rho a}\mathbf{f}\nabla\cdot\mathbf{f}. \tag{18}$$

Here and below I drop the brackets that indicate the smoothing of the energy density and flux.

The conformal transformation that eliminated the expansion of the universe in the action has the same effect here. The transformations are $\tilde{\rho} = a^4\rho$, $\tilde{\mathbf{f}} = a^4\mathbf{f}$, $d\tilde{t} = dt/a$. Without the tildes, Eqs. (13) and (18) in the new variables are

$$\begin{aligned}\frac{\partial\rho}{\partial t} &= -\nabla\cdot\mathbf{f},\\ \frac{\partial\mathbf{f}}{\partial t} &= -\frac{1}{3}\nabla\rho - \frac{1}{8\rho}\nabla f^2 - \frac{3}{4\rho}\mathbf{f}\nabla\cdot\mathbf{f}.\end{aligned} \tag{19}$$

For motion in one space dimension this becomes

$$\frac{\partial\rho}{\partial t} = -\frac{\partial f}{\partial x}, \qquad \frac{\partial f}{\partial t} = -\frac{1}{3}\frac{\partial\rho}{\partial x} - \frac{f}{\rho}\frac{\partial f}{\partial x}, \tag{20}$$

with the wave equation

$$\frac{\partial^2\rho}{\partial t^2} = \frac{1}{3}\frac{\partial^2\rho}{\partial x^2} + \frac{1}{2\rho}\frac{\partial^2 f^2}{\partial x^2}. \tag{21}$$

Eq. (19) is the weak gradient model (WGM) for the evolution of the field energy density smoothed over scales small compared to the coherence length of the energy distribution and large compared to the wavelength and period of oscillation of the field. This is a computation in second order in the perturbation from a static homogeneous energy distribution.

The first part of the WGM in Eq. (19) just expresses energy conservation after the transformation to the scaled field in Minkowski spacetime. The second part can be compared to the behavior of an ideal fluid with rest energy density ρ_r and pressure $p_r = \rho_r/3$. The components of the stress-energy tensor T^{ij} for this fluid are

$$\begin{aligned}T^{00} &= \rho = (4\gamma^2 - 1)\rho_r/3,\\ T^{0\alpha} &= f^\alpha = 4\rho_r\gamma^2 v^\alpha/3,\\ T^{\alpha\beta} &= (\delta^{\alpha\beta} + 4\gamma^2 v^\alpha v^\beta)\rho_r/3.\end{aligned} \tag{22}$$

Here α labels the spatial Cartesian coordinates. The time part of the divergence of T^{ij} is the first part of Eq. (19). The space part of the divergence, in second order perturbation theory, is

$$\frac{\partial\mathbf{f}}{\partial t} = -\frac{1}{3}\nabla\rho + \frac{1}{4\rho}\nabla f^2 - \frac{3}{4\rho}\mathbf{f}(\nabla\cdot\mathbf{f}) - \frac{3}{4\rho}(\mathbf{f}\cdot\nabla)\mathbf{f}. \tag{23}$$

If the flow is irrotational in first order perturbation theory, we can write $(\mathbf{f}\cdot\nabla)\mathbf{f} = \nabla f^2/2$ in the last term.

In this case Eq. (23) is the same as the second part of Eq. (19).

Since the evolution of the field energy distribution is the same as that of an irrotational relativistic fluid through second order in the perturbation from the static solution, the growing departure from the linear acoustic model may be expected to resemble the development of shock waves. One sees this in the WGM by considering solutions to Eq. (20) in second order perturbation theory. A standing wave solution is

$$\rho = \rho_b[1 + A\cos kx\,\cos\Omega t + A^2\cos 2kx\,(1 - \cos 2\Omega t - \Omega t\sin 2\Omega t)/8 + \ldots], \quad (24)$$

where ρ_b is the mean energy density and $\Omega = k/\sqrt{3}$. A travelling wave solution is

$$\rho = \rho_b[1 + A\sin k(x - t/\sqrt{3}) - (\Omega t A^2/4)\sin 2k(x - t/\sqrt{3}) + \ldots]. \quad (25)$$

The nonlinear correction term in Eq. (25) makes the leading part of a maximum of the energy distribution steeper than the trailing part, as in the development of a shock wave in an ideal fluid. In the standing wave solution the first nonlinear correction term vanishes when the leading term vanishes or is at a stationary point; at other times the correction term makes the extremum of the energy distribution more prominent and narrower.

IV. NUMERICAL SOLUTIONS

More detailed illustrations of the evolution of the energy distribution, and tests of the WGM, are presented in Figures 1 to 5. The solid curves are computed from numerical integration of the wave Eq. (8), and the dashed curves are from numerical solutions to the WGM in Eq. (20). In these examples the initial field amplitude is almost constant at y_o. When the length and time unit is $(\lambda^{1/2}y_o)^{-1}$, and the mean of y is scaled to unit amplitude, the field equation is

$$\partial^2 y/\partial t^2 = \nabla^2 y - y^3, \quad (26)$$

and the initial energy density is close to $\rho = 1/4$.

The numerical integration of the WGM uses the density as a function of position, rather than its mean value, in the denominator of Eq. (19), but that does not much matter because the energy density fluctuations remain small. The numerical solutions are periodic in the space intervals in the figures. The second spatial derivative is approximated as $y_i'' = (y_{i+1} - 2y_i + y_{i-1})/\delta_x^2$, where δ_x is the spatial coordinate interval, with the usual extension to two spatial dimensions. The time integration uses $y(t + \delta_t) = y(t) + 0.5\delta_t[\dot{y}(t + \delta t) + \dot{y}(t)]$, where $\dot{y}(t + \delta t)$ is computed by iteration.

The initial condition in Fig. 1 for a standing wave in one dimension is $\partial y/\partial t = 0$ with

$$y = 1 + B\sin(kx). \quad (27)$$

The amplitude of the initial field fluctuation is $B = 0.0125$, so the maximum initial density contrast is $\delta\rho/\rho = A \simeq 4B = 0.05$. The wavenumber is $k = 0.01\lambda^{1/2}y_o$, or $k = 0.01$ in the units of Eq. (26). The labels in the figure are the times from the initial condition in Eq. (27) in units of the period $T = 2\pi\sqrt{3}/k$ of oscillation of the energy distribution in a linear acoustic wave model. The numerical solutions use 700 time steps per period of oscillation of the field value at the mean amplitude y_o, or about 1×10^5 time steps in the acoustic oscillation period T. Increasing the size of the numerical time step by a factor of two or four has little effect on the energy distribution at the time $20T$ shown in the figure. At $40T$ the numerical results are sensitive to the time step; exploration of this stage of the evolution would require a more careful computation than has been attempted here. There are 350 space steps in the periodic boundary condition. If the coordinate interval is smaller than this, numerical instability spoils the integration before $20T$.

The wavelengths of the small-scale fluctuations behind the shock-like features in Fig. 1 vary with the coordinate interval δ_x; the value of the small-scale wavelength is a numerical artifact. I expect that in the limit of a continuous field the small-scale oscillations would approach the wavelength set by the period of oscillation of the field, since that and δ_x are the only relevant length scales in the computation.

The top five curves in Fig. 1 show one half oscillation in the acoustic wave model. It is notable that the shock-like features pass through each other with little interference, leaving quite smooth energy distributions behind them.

Fig. 2 shows the effect of lowering the initial amplitude B in Eq. (27) by a factor of ten and increasing the integration time by a factor of ten. As expected from Eq. (24), the time to appearance of significant departures from a linear acoustic oscillation scales inversely with the initial density contrast. It might be noted also that decreasing B increases the wavelengths of the small-scale oscillations.

Fig. 3 shows the energy distribution in a numerical solution to the wave equation in two spatial dimensions, for the purpose of checking whether the single spatial dimension in the first two examples significantly limits the nature of the departure from acoustic oscillations. The initial conditions are $\partial y/\partial t = 0$ and

$$y = 1 + B[\sin(k_x x) + \sin(k_y y)]/\sqrt{2}. \quad (28)$$

The last factor makes the rms density contrast the same as in Eq (27). The wavenumber on the horizonal axis in Fig. 3 is the same as in Fig. 1, and the wavenumber on the vertical axis is 50/77 times the horizontal wavenumber.

The energy contours are plotted at time $20T$, where T is the acoustic oscillation period for the mode running in the horizontal direction. This is the same time as for the energy distribution at the top curve in Fig. 1, and it amounts to 12.99 times the acoustic period in the vertical direction. The amplitude B is the same as in Fig. 1, and the time step is the same, but there are only 50×77 space steps. The energy distribution from the WGM is similar, though the density maximum at the lower left is narrower in the horizontal direction and the minimum at the upper right is broader.

Better spatial resolution in this two-dimensional example would give a clearer picture of the failure of the acoustic wave model but would require a more ambitious computation. One does see the departure from acoustic wave oscillation, and it appears at about the same time as in the one-dimensional examples. There is no indication in this example that the extra dimension allows qualitatively different behavior.

In an application to a model for structure formation in cosmology [3], small-scale shock-like features the in y-field energy distribution could appear well before density fluctuations of interest to astronomy reach the Hubble length. Fig. 4 shows a check of the effect on the acoustic wave model for the large-scale energy distribution. The initial conditions are $\partial y/\partial t = 0$ and

$$y = 1 + B[\sin(kx) - \sin(8kx)]. \tag{29}$$

The parameters in the numerical integration are the same as in Fig. 1.

At time $t = 2T$, at two acoustic oscillation periods of the long wavelength mode in Fig. 4, the short wavelength mode has completed 16 oscillations and the cascade to shorter wavelengths is commencing. At $t = 5T$ the large-scale energy distribution is still close to the original sine wave, consistent with the acoustic wave model. This decoupling from the nonlinear small-scale behavior is familiar from other fluid models, and might be expected here on roughly similar grounds. In a region where the smoothed energy density is larger than average the y-field generally is oscillating more rapidly than average. That produces a gradient in the phase of the field oscillation that produces a flux of energy away from this region. Local nonlinear features produce local fluctuations in the phase gradient but have little effect on its mean or on the mean energy flux density.

Finally, a travelling wave solution offers a clearer illustration of the formation of shock-like features. The initial condition for the one-dimensional sinusoidal travelling wave in Fig. 5 is

$$\begin{aligned} y(x,t) &= (1+\dot{\phi})\eta(t+\phi), \\ \dot{\phi} &= B\cos k(x - t/\sqrt{3}), \end{aligned} \tag{30}$$

where $\eta(t)$ is a solution for the quartic oscillator with unit amplitude in Eqs. (2) and (3). Eq. (30) is a solution to the wave Eq (26) if terms of order B^2 and kB may be ignored. I use a numerical solution for $\eta(t)$, with $\eta = 1$ and $\dot{\eta} = 0$ at $x = 0$ in Eq. (30). This phase choice does not matter because η oscillates much more rapidly than the energy distribution. The amplitude B and the other parameters in the computation are the same as in the standing wave example in Fig. 1. The growing departure from an acoustic oscillation looks very much like the development of a shock wave, as in Eq. (25). The time to development of large departures from the acoustic model is about half that of the standing wave, as might be expected from the larger correction term in Eq. (25) and the coherence of phases of the leading and correction terms in the travelling wave. The length of the train of oscillations behind the shock-like feature doubles from time $10T$ to $20T$. At $40T$ short wavelength oscillations in the energy density in the numerical solution fill space, in a complicated pattern of amplitude and wavelength fluctuations. This part of the evolution is not to be trusted, however, because the details are sensitive to the size of the space step in the computation.

V. CONCLUDING REMARKS

The discussion in Sec. II shows that under the initial conditions assumed here the initial departure from a homogeneous energy distribution starts to rearrange itself in the manner of an ideal relativistic fluid with pressure $p_r = \rho_r/3$. Not so evident is that as the phase of the field oscillation as a function of position winds and unwinds the energy distribution continues to behave like a fluid. This behavior follows in the weak gradient model in Sec. III (Eq. 19). The weak gradient model in turn is equivalent to the equation of motion of a relativistic fluid to second order in the perturbation from a homogeneous energy distribution, provided the flow is irrotational in first order perturbation theory.

In the numerical tests in Figs. 1 to 5 the weak gradient model agrees well with the energy distribution obtained from numerical solutions of the wave equation. That is, we have good evidence for the picture of how the near acoustic wave behavior of the energy distribution ends: features that resemble shock waves appear after a time on the order of

$$\tau_{\rm nl} \sim T/\delta\rho/\rho, \tag{31}$$

where T is the oscillation time in the acoustic model and the rms density contrast is $\delta\rho/\rho$.

The features are not true shock waves, of course. In particular, they excite energy fluctuations in a reversible way: the field returns to a smooth energy distribution after the feature has passed by. There is no artificial viscosity in the computation, and I have not been able to see how the effect could be a numerical artifact; this

seems to be real reversible process. The near elastic interactions illustrated in the half cycle in Fig. 1 remind one of solitions, but this behavior has a limited lifetime: the length of the train of oscillations behind the leading edge increases with time.

More ambitious analyses than have been attempted here would be needed to explore the evolution of the shock-like features. If, as seems likely, the fluctuations in the spatial distribution of the field energy eventually cascade to noise extending to wavenumbers comparable to the frequency ω of the field oscillation (Eq. 4), the energy distribution may be expected to end up behaving like a gas of interacting particles with de Broglie wavenumber on the order of ω [9]. The near fluid behavior on scales much larger than the de Broglie wavelength might still obtain, however, because the gas has a short mean free path. This aspect of the evolution remains to be analyzed.

VI. ACKNOWLEDGMENTS

This work has benefitted from discussions with Andrei Gruzinov, Wayne Hu, and Alex Vilenkin, and was supported in part at the Institute for Advanced Study by the Alfred P. Sloan Foundation and at Princeton University by the National Science Foundation.

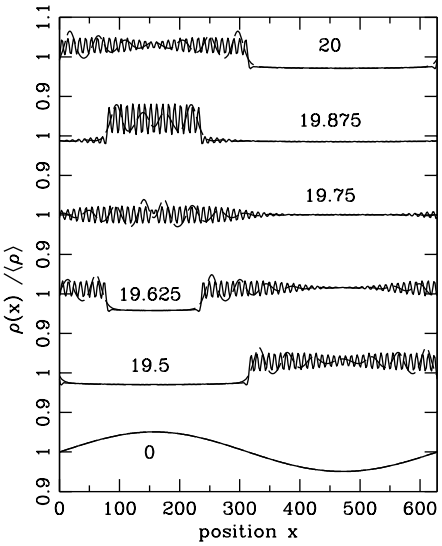

FIG. 1. Evolution of a one-dimensional standing wave in the energy distribution of a field with a quartic self-interaction potential. The solid lines are from a numerical integration of the wave equation (Eq. 26), and the dashed lines are a numerical solution of the weak gradient model (Eq. 20). The energy distributions are plotted at the indicated multiples of the period of oscillation of the initial sine wave in the linear acoustic wave model.

[1] P. J. E. Peebles & A. Vilenkin, Phys. Rev. **D59**, 063505 (1999).
[2] P. J. E. Peebles & A. Vilenkin, Phys. Rev., in press, astro-ph/9904396.
[3] W. Hu & P. J. E. Peebles, astro-ph/9910222
[4] L. H. Ford, Phys. Rev. D **35**, 2955 (1987).
[5] M. S. Turner, Phys. Rev. **D28**, 1243 (1983).
[6] G. Felder, L. Kofman and A. D. Linde, hep-ph/9903350.
[7] M. Yu. Khlopov, B. A. Malomed, and Ya. B. Zel'dovich, M. N. R. A. S. **215**, 575 (1985).
[8] S. Yu. Khlebnikov & I. I. Tkachev, Phys. Rev. Lett. **77**, 219 (1996).
[9] A. Gruzinov, private communication.
[10] P. B. Greene, L. Kofman, A. Linde, & A. A. Starobinsky, Phys. Rev. **D 56**, 6175 (1997).
[11] A. A. Starobinsky and J. Yokoyama, Phys. Rev. **D 50**, 6357 (1994).
[12] A. Vilenkin, private communication.

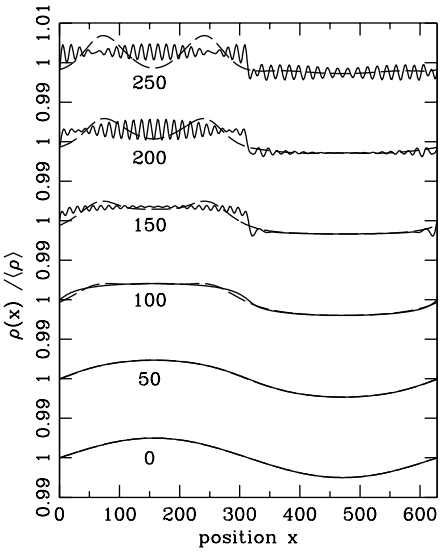

FIG. 2. Illustration of the effect of decreasing the wave amplitude in Fig. 1 by a factor of ten. The curves are plotted at the indicated multiples of the acoustic oscillation time. All other parameters are the same as in Fig. 1.

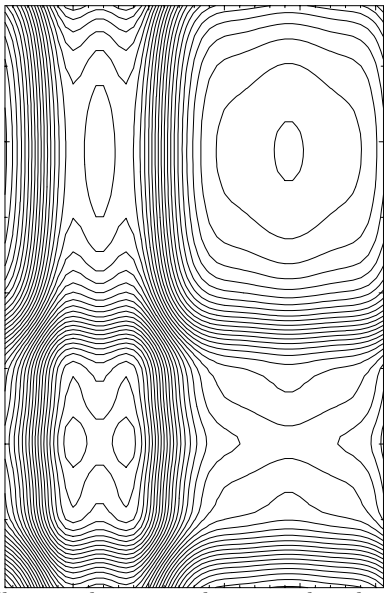

FIG. 3. The two-dimensional energy distribution after 20 times the period for an acoustic oscillation in the horizontal direction. This is 13 times the acoustic oscillation period in the vertical direction. The energy distribution is from a numerical integration of the field equation with the initial condition in Eq. (28). The time step, amplitude parameter B, and wavenumber in the horizontal direction are the same as in Fig. 1, but the spatial resolution is worse by a factor of seven. The highest density contours, in the two peaks at the lower left, are at contrast $\delta\rho/\rho = 0.069$; the lowest contour, at $\delta\rho/\rho = -0.045$, is at the upper right. The nearly flat regions in the upper left and lower right are at close to zero density contrast.

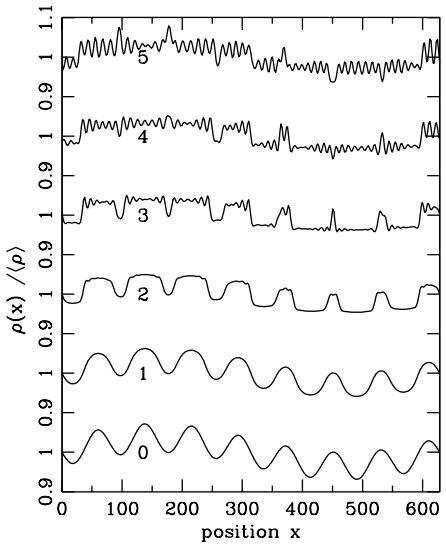

FIG. 4. Illustration of the effect of small-scale nonlinear fluctuations on evolution of the mass distribution on larger scales. The initial condition is in Eq. (29). At the time of the top curve the long wavelength component has oscillated five times and the short wavelength component 40 times in the acoustic wave model. The other parameters are the same as in Fig. 1.

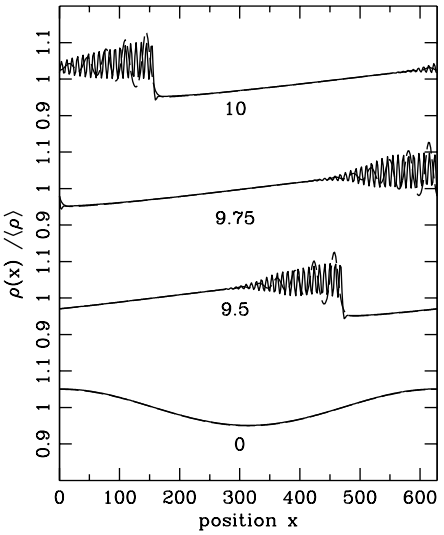

FIG. 5. A travelling wave solution with the initial condition in Eq. (30). All other parameters are the same as in Fig. 1.